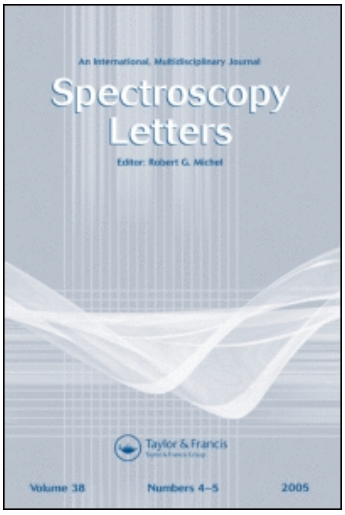

Spectroscopy Letters
Publication details, including instructions for authors and subscription information:
http://www.informaworld.com/smpp/title~content=t713597299

Luminescence of $Cs_2NaScCl_6:Pr^{3+}$: Effects of Changing the Elpasolite Lattice Parameter

X. -J. Zhou[a]; P. A. Tanner[b]; M. D. Faucher
[a] Institute of Modern Physics, Chongqing University of Post and Telecommunications, Chongqing, China [b] Department of Biology and Chemistry, City University of Hong Kong, Kowloon, Hong Kong S.A.R., People's Republic of China

To cite this Article Zhou, X. -J. , Tanner, P. A. and Faucher, M. D.(2007) 'Luminescence of $Cs_2NaScCl_6:Pr^{3+}$: Effects of Changing the Elpasolite Lattice Parameter', Spectroscopy Letters, 40: 2, 349 — 366
To link to this Article: DOI: 10.1080/00387010701247720
URL: http://dx.doi.org/10.1080/00387010701247720

Spectroscopy Letters, 40: 349–366, 2007

ISSN 0038-7010 print/1532-2289 online
DOI: 10.1080/00387010701247720

Luminescence of $Cs_2NaScCl_6:Pr^{3+}$: Effects of Changing the Elpasolite Lattice Parameter

X.-J. Zhou
Institute of Modern Physics, Chongqing University of Post and Telecommunications, Chongqing, China

P. A. Tanner
Department of Biology and Chemistry, City University of Hong Kong, Kowloon, Hong Kong S.A.R., People's Republic of China

M. D. Faucher
88 Avenue Jean Jaures, 92140, Clamart, France

Abstract: The luminescence spectrum of $Cs_2NaScCl_6:Pr^{3+}$ (0.1 at.%) has been recorded at temperatures down to 10 K and assigned between 20,800 and 9900 cm^{-1}. Twenty-three energy levels of the $4f^2$ configuration Pr^{3+} ion were located and then fitted by the conventional $4f^2$ crystal field calculation, as well as by a configuration interaction assisted crystal field (CIACF) calculation. The latter gave a much better fit. A comparison of the fit for $Cs_2NaScCl_6:Pr^{3+}$ with fits upon the same set of energy levels in $Cs_2NaYCl_6:Pr^{3+}$ and $Cs_2NaPrCl_6$, where the fifth nearest neighbor of Pr^{3+} is changed and the lattice parameter increases along this series, shows a decrease in the magnitudes of the crystal field parameters, which were also semiquantitatively simulated. Several facets of the emission spectra are interesting, including the observation of weak progressions in the totally symmetric Pr–Cl stretching vibration and the occurrences of the resonance of electronic and vibronic states. The spectra of $Cs_2NaScCl_6:Pr^{3+}$ (1 at.%) differ considerably from those of

Received 28 May 2006, Accepted 24 August 2006
The authors were invited to contribute this paper to a special issue of the journal entitled "Spectroscopy of Lanthanide Materials." This special issue was organized by Professor Peter Tanner, City University of Hong Kong, Kowloon.
Address correspondence to P. A. Tanner, Department of Biology and Chemistry, City University of Hong Kong, Tat Chee Avenue, Kowloon, Hong Kong S.A.R., People's Republic of China. E-mail: bhtan@cityu.edu.hk

the more dilute system and show that other species are formed rather than a complete substitution of the Sc^{3+} sites by Pr^{3+}.

Keywords: Configuration interaction, crystal field, electronic spectra, lanthanide

INTRODUCTION

$Cs_2NaScCl_6$ has often been employed as a transparent host lattice for the study of activator ion luminescence. It crystallizes in the *Fm3m* space group, and the Sc^{3+} ion occupies an octahedral symmetry site.[1] Thus the luminescence of As(III),[2] Rh^{3+},[3] and Cr^{3+}[4,5] have been investigated in the $Cs_2NaScCl_6$ host crystal. Figure 1 shows a schematic diagram of the general elpasolite crystal lattice M_2ALnX_6 and the coordination geometry about Ln^{3+}. The relevant internuclear separations for some specific systems are listed in Table 1. More recently, V^{3+}-sensitized upconversion of Pr^{3+} has been investigated in the $Cs_2NaScCl_6$ host.[6] This caught our attention because we have studied the configuration interaction (CI) of Pr^{3+} in elpasolite hosts, including the investigation of its optical spectra.[7] The energy levels for the $4f^2$ Pr^{3+}

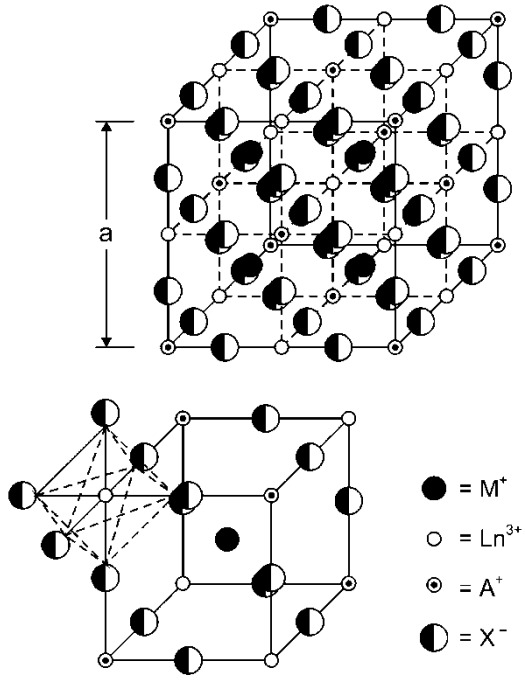

Figure 1. Schematic diagram of the M_2ALnX_6 (M = Cs; A = Na; Ln = Sc or lanthanide ion; X = Cl) elpasolite crystal lattice, also showing the octahedral coordination geometry of Ln. a is the lattice parameter.

Table 1. Distance to nearest neighbors (pm) in $Cs_2NaPrCl_6$, Cs_2NaYCl_6: Pr^{3+} and $Cs_2NaScCl_6$: Pr^{3+}

Neighbor	Number of neighbors	$Cs_2NaPrCl_6$	Cs_2NaYCl_6: Pr^{3+}	$Cs_2NaScCl_6$: Pr^{3+}
Chlorine	6	268.4	264.0	258.0
Cesium	8	472.5	464.8	454.1
Sodium	6	545.6	536.7	524.4
Chlorine	24	612.0	602.0	588.2
Lanthanide	12	771.6	758.9	741.6

system are described by the notation $^{2S+1}L_J\ \Gamma_i$ ($i = 1...5$), where the irreducible representation Γ_i refers to the (gerade) irreducible representation in the O_h molecular symmetry point group. We noticed that the energy given in Ref. 6 for the lowest $^1G_4$ level is rather different from that in other elpasolite hosts,[7] so that the $Cs_2NaScCl_6$ lattice might serve as a further test concerning the importance of CI for the $4f^2$ configuration. Indeed, the ionic radius of Sc^{3+} (75 pm) is rather smaller than that of Pr^{3+} (99 pm) so that doping Pr^{3+} into the lattice should lead to a much stronger crystalline field. Thus, we present the optical emission spectra in this paper and use this data for crystal field calculations with and without the inclusion of CI. For comparison, we also refer to data for $Cs_2NaLnCl_6$:Pr^{3+} (Ln = Pr, Y, Gd) where the identity of the fifth nearest neighbor differs.

MATERIALS AND METHODS

$Cs_2NaScCl_6$:Pr^{3+} (0.1 and 1.0 at.%) were prepared as powders by Morss method E[8] and then passed *in vacuo* through a Bridgman furnace at 850°C. Emission spectra were recorded at resolution of 2–4 cm^{-1} by an Acton 0.5-m monochromator having a 1200 grooves mm^{-1} grating blazed at 500 nm, and a back-illuminated SpectruMM CCD detector, using an optical parametric oscillator (OPO; Panther) pumped by the third harmonic of a Surelite Nd:YAG pulsed laser. The sample was housed in an Oxford Instruments closed-cycle cryostat. The survey excitation spectra were recorded by scanning the OPO and detecting the emission by a Hamamatsu R928 photomultiplier tube.

RESULTS AND DISCUSSION

Description of Emission Spectra: Luminescence of $Cs_2NaScCl_6$:Pr^{3+} (0.1 at.% Pr)

The analysis of the optical spectra of Pr^{3+} in elpasolite hosts and the detailed band assignments have previously been described (refer to Ref. 7 and

references therein) so that we briefly present the interesting features and salient differences here because the assignments for the current spectra are consistent with those published. The electronic spectra are mainly vibronic in character, with each transition having an electric quadrupole or magnetic dipole allowed zero phonon line accompanied by a one (ungerade) moiety-mode phonon sideband and lattice vibration structure. Vibrational data for the $Cs_2NaScCl_6$ host from Raman spectroscopy, and vibronic data for Pr^{3+} in this host lattice and in $Cs_2NaPrCl_6$, are presented in Table 2. The Pr–Cl and Na–Cl bond frequencies are both higher in $Cs_2NaScCl_6$:Pr^{3+} than in $Cs_2NaPrCl_6$, and this is shown in Figure 2 where these bond stretching energies from vibronic data are plotted against the lattice parameters of crystals in which Pr^{3+} is doped. The crystals with smaller lattice parameter exhibit higher stretching frequencies.

The emission spectra of $Cs_2NaScCl_6$:Pr^{3+} are well resolved. Under blue laser excitation, the luminescent state is the nondegenerate $^3P_0\Gamma_1$ state at 20,576 cm^{-1}. Figures 3a–3f show the 470-nm excited spectra at 10 K and 77 K. The 446-nm excited spectra are similar. The multiplet term transitions and (inferred) locations of terminal crystal field states are marked in the figure in addition to the prominent vibronic structure. All bands in the figure have been assigned. The derived energy levels of the terminal states are listed in Table 3 in the Exp column of $Cs_2NaScCl_6$:Pr^{3+}.

The vibronic structure to low energy of the zero phonon lines in the spectra of this dilute material mostly comprises single sharp bands, with the exception of S_{10} ν_6 where a strong and a weaker band are observed at 79

Table 2. Vibrational structure in the Raman and electronic spectra of Pr^{3+} in crystals at 10–20 K

	Raman (R) or vibronic data (cm^{-1})		
Mode and symmetry[a]	$Cs_2NaScCl_6$[4,9]	$Cs_2NaPrCl_6$	$Cs_2NaScCl_6$:Pr^{3+}
S_1 ν_1 α_{1g} M–Cl str.	294 (R)	282 (R)	310
S_2 ν_2 ε_g M–Cl str.	212 (R)	220 (R)	—
S_5 τ_{2g} Cs^+ lattice	52 (R)	37, 40	51
S_6 ν_3 τ_{1u} M–Cl str.	—	235, 245, 276	277
S_7 ν_4 τ_{1u} Cl–M–Cl b.	—	98, 113, 120	103
S_8 τ_{1u} Na–Cl str.	—	172, 183	213
S_9 τ_{1u} Cs^+ transl.	—	58	61
S_4 ν_5 τ_{2g} Cl–M–Cl b.	147 (R)	114 (R)	—
S_{10} ν_6 τ_{2u} Cl–M–Cl b.	—	72–82	70, 79

transl., translation; str., stretch; b., bend. M is Pr or Sc.

[a]Refer to the unit cell group notation in Ref. 10. The multiple structures for each vibrational mode in $Cs_2NaPrCl_6$ are due to the effects of dispersion and transverse-longitudinal mode splittings.

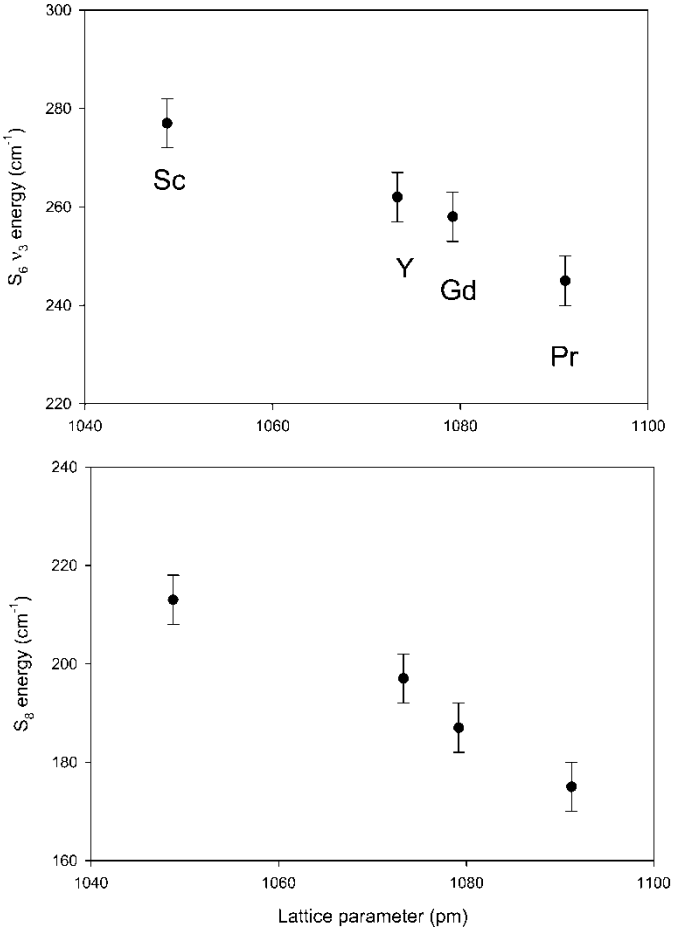

Figure 2. Variation of the Pr–Cl (S_6, ν_3) and Na–Cl (S_8) antisymmetric stretching frequency energies from vibronic data in $Cs_2NaMCl_6:Pr^{3+}$.

and 70 cm^{-1}, respectively. The zone boundary component of S_6 ν_3, which is prominent in the spectra of $Cs_2NaPrCl_6$, appears very weak in Figure 3, at 233 cm^{-1} to low energy of each electronic origin. These changes in the spectra of $Cs_2NaScCl_6:Pr^{3+}$ versus those of $Cs_2NaPrCl_6$ reflect the absence of phonon dispersion and transverse-longitudinal mode splittings in the dilute material.

Two further points resulting from the analysis of the spectra are of interest. First, the progressions in the totally symmetric Pr–Cl stretching mode, $S_1\nu_1$, can be observed clearly in several transitions. It is not generally accepted that there are slight bond length changes in the $4f^N$ excited states of lanthanide ions, relative to the electronic ground state. In Figure 3a, the first members of the vibrational progressions in S_1 on the vibronic structure of $^3P_0\Gamma_1 \rightarrow (^3H_4)$

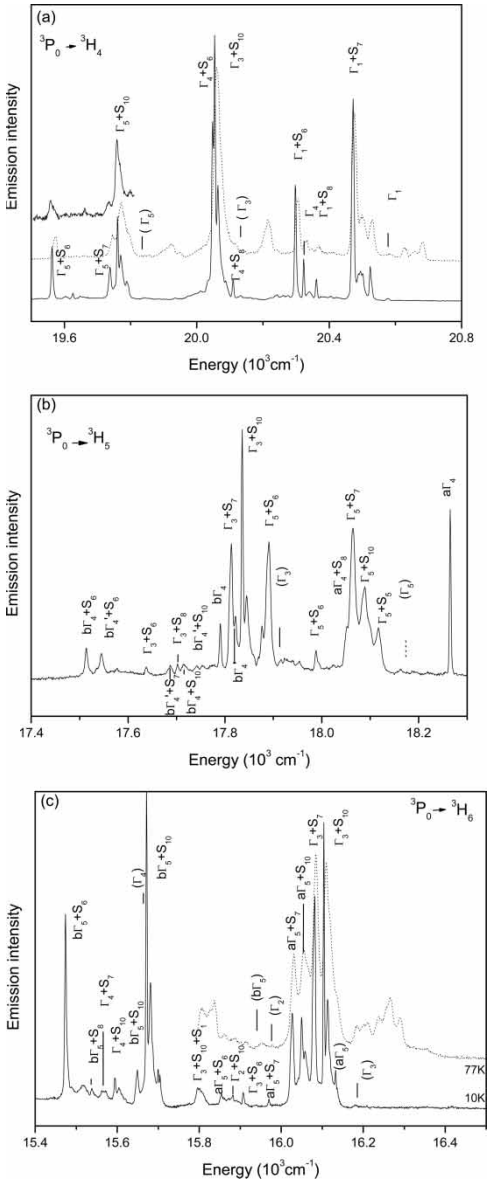

Figure 3(a)–(f). Excited (470 nm) 10 K and 77 K $^3P_0\Gamma_1$ emission spectra of $Cs_2NaScCl_6:Pr^{3+}$ (0.1 at.% Pr^{3+}). The terminal crystal field electronic and vibronic states are marked. In (a), the upper left-hand line has been displaced to low energy by 310 cm^{-1}. In (b), the $b\Gamma_4$ and $b\Gamma'_4$ states are electron–phonon coupled $b\Gamma_4$ and $\Gamma_3 + S_4$ states, and in (d) the Γ_5 and Γ'_5 states are coupled Γ_5 and $\Gamma_3 + S_4$ states, respectively.

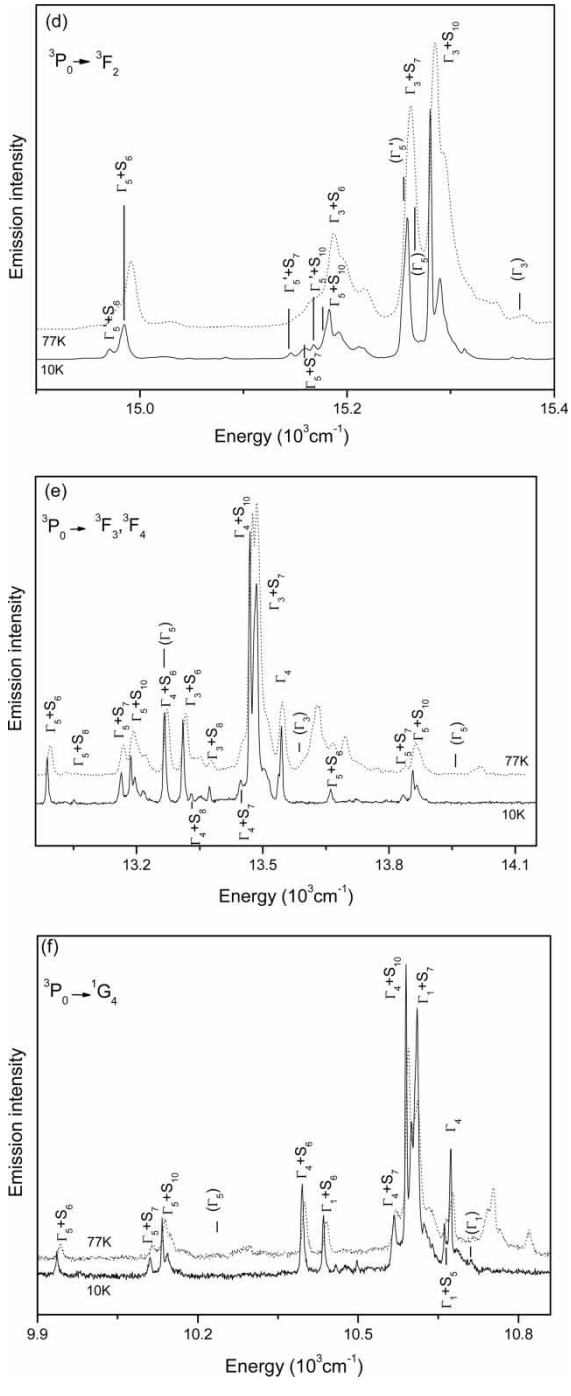

Figure 3(a)–(f).

Table 3. Energy level calculations for Pr^{3+} in elpasolite lattices

			$Cs_2NaPrCl_6$			$Cs_2NaYCl_6:Pr^{3+}$			$Cs_2NaScCl_6:Pr^{3+}$		
				Calc.			Calc.			Calc.	
N	Level	Label	Exp.	$4f^2$	$4f^2 + 4f6p$	Exp.	$4f^2$	$4f^2 + 4f6p$	Exp.	$4f^2$	$4f^2 + 4f6p$
1	$^3H_4$	Γ_1	0	51	8	0	47	5	0	50	8
2	$^3H_4$	Γ_4	242	263	246	245	266	251	252	277	257
3	$^3H_4$	Γ_3	422	410	411	435	418	423	442	436	430
4	$^3H_4$	Γ_5	702	673	719	724	684	734	735	705	748
5	$^3H_5$	aΓ_4	2300	2313	2296	2303	2317	2301	2311	2327	2305
6	$^3H_5$	Γ_5	2399	2414	2395	2404	2420	2401	2408	2433	2404
7	$^3H_5$	Γ_3	2645	2617	2649	2653	2625	2658	2661	2638	2668
8	$^3H_5$	bΓ_4	2763	2706	2749	2773	2719	2763	(2766)	2738	2774
9	$^3H_6$	Γ_3	4386	4406	4373	4385	4409	4374	4391	4414	4375
10	$^3H_6$	aΓ_5	4437	4454	4429	4441	4459	4431	4445	4466	4434
12	$^3H_6$	Γ_2	4591	4636	4617	4606	4648	4627	4613	4666	4628
13	$^3H_6$	bΓ_5	4807	4786	4808	4815	4795	4815	4823	4808	4822

14	$^3H_6$	Γ_4	4881	4853	4887	4890	4864	4897	4901	4878	4905
11	$^3H_6$	Γ_1	—	4884	4922	—	4894	4932	—	4908	4941
15	$^3F_2$	Γ_3	5203	5231	5193	5206	5234	5196	5215	5246	5196
16	$^3F_2$	Γ_5	5297	5286	5305	5305	5291	5313	5316	5305	5316
17	$^3F_3$	Γ_4	—	6633	6603	—	6637	6606	—	6648	6608
18	$^3F_3$	Γ_5	6621	6640	6621	6625	6645	6624	6648	6658	6628
19	$^3F_3$	Γ_2	—	6992	6705	—	6697	6709	—	6709	6712
22	$^3F_4$	Γ_1	—	6917	6907	—	6924	6913	—	6739	6929
20	$^3F_4$	Γ_3	6965	6997	6984	6973	7001	6987	6999	7011	7005
21	$^3F_4$	Γ_4	7012	6971	6980	7015	6976	6986	7043	6988	7003
23	$^3F_4$	Γ_5	7278	7255	7271	7288	7265	7280	7322	7283	7299
24	$^1G_4$	Γ_1	9847	9777	9843	9853	9783	9850	9874	9793	9877
25	$^1G_4$	Γ_4	9895	9856	9900	9890	9861	9902	9914	9868	9931
26	$^1G_4$	Γ_3		9902	9924		9906	9922	—	9909	9952
27	$^1G_4$	Γ_5	10,327	10,420	10,333	10,340	10,441	10,338	10,373	10,466	10,367
28	$^1D_2$	Γ_5		16,761	16,681		16,742	16,662	—	16,730	16,624
29	$^1D_2$	Γ_3		17,247	17,255		17,240	19,249	—	17,241	17,221
30	$^3P_0$	Γ_1	20,625	20,626	20,627	20,600	20,600	20,601	20,576	20,585	20,583

$\Gamma_5 + S_i$ ($i = 6, 8, 7, 10$) are shown as an upper left-hand full line that is shifted to low energy by 310 cm^{-1}. The progressions are about 1/40 as intense as the vibronic structure that they are based on. The Pr–Cl distance is 258 pm in this lattice, and its change in bond distance for these intraconfigurational transitions is however quite small and is calculated by Franck–Condon analysis[10] to be 0.7 pm.

The second point concerns the resonance between electronic and vibronic levels that has previously been observed for Yb^{3+} and Tm^{3+} systems.[10] In fact, a resonance of this type was reported for the $^3P_0\Gamma_1 \rightarrow {}^3F_2$ transition of $Cs_2NaYCl_6:Pr^{3+}$,[11] where the $\Gamma_1 \rightarrow a\Gamma_4 + S_4 + S_i$ transitions were essentially coincident with $\Gamma_1 \rightarrow \Gamma_5 + S_i$ and gained intensity by Fermi resonance. In the current case, the resonances marked in Figure 3b occur for the same $^3P_0\Gamma_1 \rightarrow {}^3H_5$ transition but are between $\Gamma_1 \rightarrow \Gamma_3 + S_4 + S_i$ and $\Gamma_1 \rightarrow b\Gamma_4 + S_i$ so that a doubling of bands in the transitions terminating upon $b\Gamma_4$ electronic and vibronic states appears. These electron-phonon coupled states are labeled $b\Gamma_4$ and $b\Gamma_4'$. From the resonance, the energy of the S_4 vibration of Pr^{3+} in $Cs_2NaYCl_6:Pr^{3+}$ is estimated to be between 105 and 110 cm^{-1}. The separation of the "doublets" in Figure 3b is 31 cm^{-1}. The energy of the $b\Gamma_4$ electronic state has been roughly corrected for Fermi resonance in Table 3. The fact that this band doubling is not due to a static lowering of octahedral site symmetry of $PrCl_6^{3-}$ is evident from the absence of splittings of the zero phonon lines for transitions terminating upon degenerate crystal field levels, such as $\Gamma_1 \rightarrow a\Gamma_4$ in Figure 3b. A similar resonance phenomenon occurs for the $^3P_0\Gamma_1 \rightarrow {}^3F_2$ transition. Although the displacement energy is appropriate, the lowest energy band in Figure 3d is too intense to be assigned to $\Gamma_1 \rightarrow \Gamma_3 + S_{10} + S_1$, and other weaker bands are unassigned unless we consider the resonance between $\Gamma_3 + S_4 + S_i$ and $\Gamma_5 + S_i$. In this case, the splitting of the doublets is 14 cm^{-1}, and the energy of the moiety bending mode ν_5 S_4 is inferred to be $\sim$105 cm^{-1}.

Finally, the effects upon two of the energy levels of Pr^{3+} upon changing the fifth nearest neighbor in $Cs_2NaLnCl_6:Pr^{3+}$ are shown graphically in Figure 4. In effect, such changes vary the lattice parameter of the unit cell. The $^3H_4\Gamma_5$ crystal field level increases in energy with the lattice parameter decrease and consequent increase in the crystal field interaction within the $^3H_4$ multiplet term. On the other hand, the $^3P_0\Gamma_1$ energy decreases along the same series so that the luminescence from this multiplet term can be tuned slightly in wavelength by changing the fifth nearest neighbor of Pr^{3+}.

Luminescence of $Cs_2NaScCl_6:Pr^{3+}$ (1 at.% Pr)

One of the motivations for studying the $Cs_2NaScCl_6:Pr^{3+}$ system was that the excited state absorption spectrum from $^1G_4$ was previously reported by Reinhard et al.[6] We imagined that this information would be invaluable in assigning the $^1I_6$ and $^3P_{0,1,2}$ energy levels of Pr^{3+} and thereby enable a

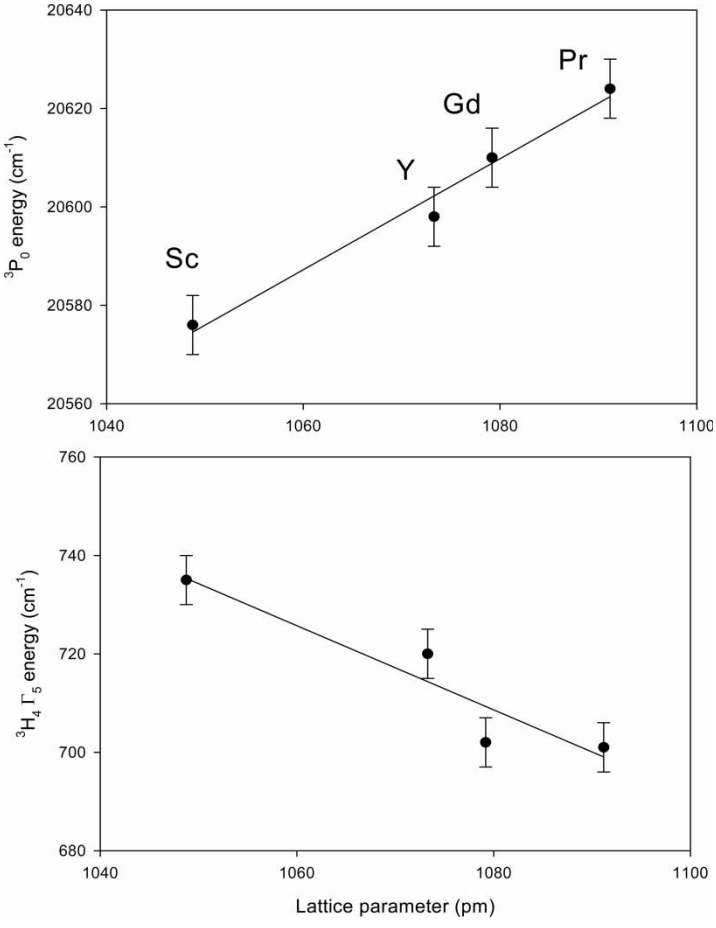

Figure 4. Effects of changes in lattice parameter in $^3P_0\Gamma_1$ and $^3H_4\Gamma_5$ energy levels as a function of lattice parameter in $Cs_2NaMCl_6:Pr^{3+}$ (Ln = Sc, Y, Gd, Pr). The regression lines are drawn as a guide to the eye.

complete energy level data set to be achieved. However, the comparison of our emission spectrum of $Cs_2NaSc_{0.999}Pr_{0.001}Cl_6$ (Figs. 3a–3d) with the 15 K emission spectrum of $Cs_2NaSc_{0.96}Pr_{0.02}V_{0.02}Cl_6$ (Fig. 2a in Ref. 6) shows that they are very different, even taking into account the lower resolution of the latter spectrum. For example, the latter $^3P_0 \rightarrow {}^3H_4$ emission spectrum has a strong peak at 20,423 cm^{-1} and two much weaker bands at 20,105, 20,014 cm^{-1}. We therefore decided to investigate the concentration dependence of the spectrum. Figure 5a compares the room temperature $^3P_0 \rightarrow {}^3H_4$ emission spectra of nominally 0.1 at.% and 1 at.% Pr^{3+}-doped $Cs_2NaScCl_6$ crystals. The 0.1 at.% Pr^{3+} spectrum comprises vibronic structure with associated hot bands, and the major transitions are marked. The 1 at.% Pr^{3+} spectrum is similar except

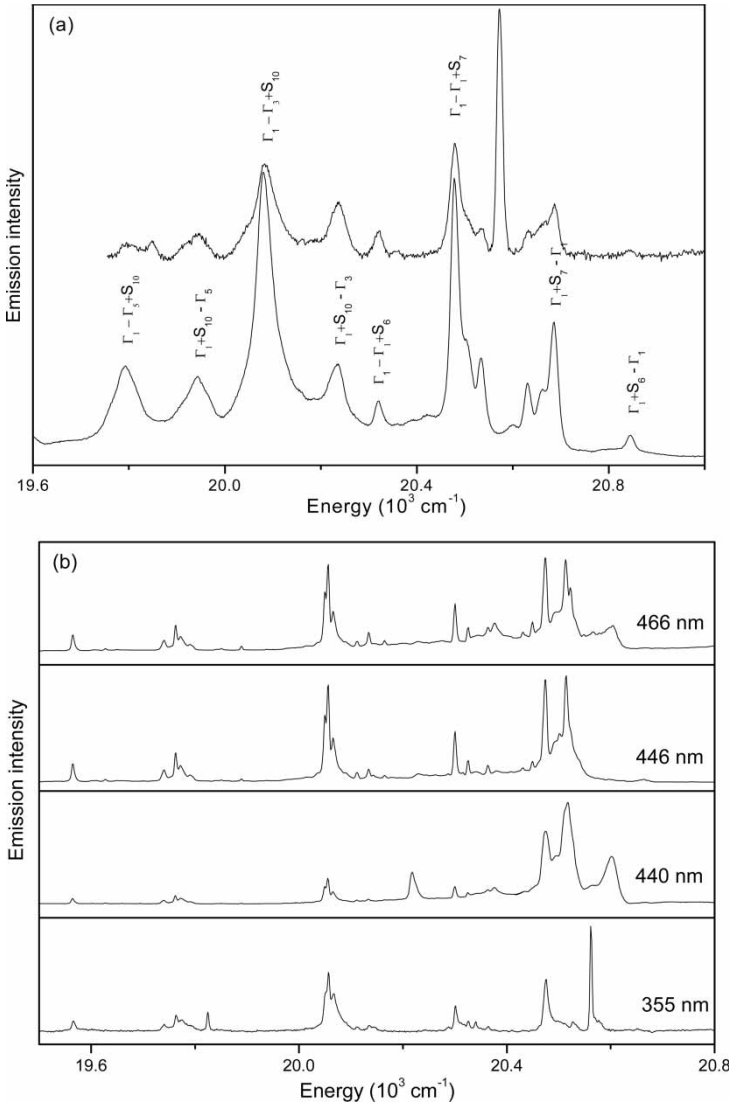

Figure 5. $^3P_0 \rightarrow {}^3H_4$ emission spectra of Pr^{3+}-doped $Cs_2NaScCl_6$. (a) Comparison of room temperature spectra of nominally 0.1 at.% and 1.0 at.% Pr^{3+}-doped crystals under 450 nm and 355 nm excitation, respectively. (b) Excitation line dependence of the spectra of 1.0 at.% Pr^{3+}-doped crystals at 10 K.

for an intense band at 4 cm^{-1} to low energy of the expected position of the $\Gamma_1 \rightarrow \Gamma_1$ electronic origin. This intense band is the zero phonon line of another lower symmetry Pr^{3+} species, which is noncentrosymmetric and can acquire electric dipole transition intensity. It is interesting that the other

electronic origins $\Gamma_1 \rightarrow \Gamma_4, \Gamma_3, \Gamma_5$ do not exhibit similar intensity enhancements. Figure 5b shows the 10 K spectra of the 1 at.% sample under different excitation lines, and although some bands are similar to those in Figure 3a, there are significant differences especially between 20,400 and 20,600 cm^{-1}. These additional bands show a pronounced excitation line–relative intensity dependence. We therefore conclude that at higher dopant levels than 0.1 at.% Pr^{3+}, some new species are formed and this is the reason why the spectra of Ref. 6 differ from that in Figure 3a.

Survey excitation spectra were recorded for the two samples with different Pr^{3+} dopant ion concentrations by monitoring the intense $^3P_0 \rightarrow {}^3F_2$ emission at 15,280 cm^{-1}. The results (Fig. 6) emphasize the differences in composition. For the 0.1 at.% sample, the decay of luminescence from $^3P_0$ was fitted to a monoexponential model, and the e^{-1} decay lifetime at 300, 77, and 10 K was 0.57, 0.73, and 0.85 ms, respectively.

CALCULATIONS OF ENERGY LEVELS AND DERIVED PARAMETERS

The electronic structure of Pr^{3+} in $Cs_2NaPrCl_6$ and Cs_2NaYCl_6: Pr^{3+} was measured and interpreted in detail in Ref. 7. Thirty eight and 36 experimental energy levels respectively were available out of the 40 in the $4f^2$ Pr^{3+}

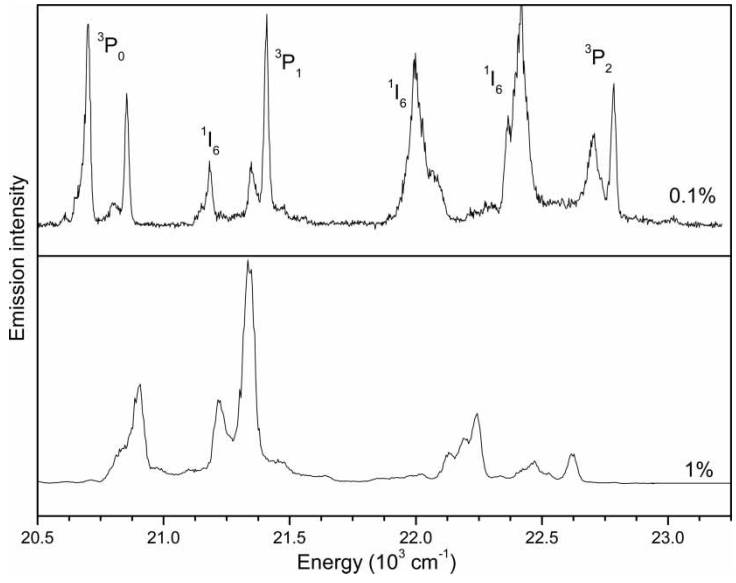

Figure 6. Survey 10 K $^3P_0 \rightarrow {}^3F_2$ excitation spectra of 0.1 and 1.0 at.% Pr^{3+}-doped $Cs_2NaScCl_6$ samples. The multiplet terms are marked for the 0.1 at.% sample.

configuration. Two methods were employed for the crystal field fitting: a standard method in $4f^2$ and a CIACF (configuration interaction assisted crystal field) fitting in which both the $4f^2$ and 4f6p configurations were diagonalized simultaneously. That operation resulted in a dramatic improvement of the fitting so that the mean deviation was divided by 2.9. The current work compares $Cs_2NaScCl_6$: Pr^{3+} with the other two isostructural systems. For the comparison to be meaningful, the fittings must utilize the same energy level set for the three materials. The data sets were therefore limited to the 23 observed levels in $Cs_2NaScCl_6$:Pr^{3+}, and the fittings were run anew for the three materials on this truncated basis. The very small number of levels forbids the fitting of all the Hamiltonian parameters, which were therefore chosen to start from the $Cs_2NaPrCl_6$ parameter set. The variation of the Slater parameter F^4 was ineffective in $4f^2$ but indispensable for $Cs_2NaScCl_6$:Pr^{3+} in ($4f^2 + 4f6p$). Thus, for the sake of comparison, it was adjusted for the three compounds. The other varying parameters in $4f^2$ were: the mean energy of the configuration E_{avg}, F^2, the crystal field parameters B_0^4 (ff) and B_0^6 (ff) (with $B_4^4 = \pm B_0^4\,(5/14)^{1/2}$, $B_4^6 = \mp B_0^6\,(7/2)^{1/2}$], and also B_0^4 (fp) when the CIACF is utilized. Varying the spin-orbit coupling constant was ineffective. All other parameters were held constant and they are given in the legend of Table 4. In the course of the fitting by CIACF, it was observed that the ratio between B_0^4 (fp) and B_0^4 (ff) was very close to 8.5 and it was subsequently held constant. The number of parameters then amounted to four in the normal $4f^2$ fit and five in the CIACF fitting. The experimental and calculated energies are reported in Table 3 and the fitted parameters in Table 4. The mean deviations are 3.1, 3.5, and 2.7 times lower when utilizing CIACF instead of the standard method for $Cs_2NaPrCl_6$, Cs_2NaYCl_6:Pr^{3+}, and $Cs_2NaScCl_6$: Pr^{3+}, respectively.

The lattice parameter is equal to 1091.2, 1073.3 and 1048.8 pm for the above three cubic systems, respectively. As mentioned before, Figure 1 shows the structure and Table 1 gives the number of neighbors and the distances to these, up to 800 pm. Six chloride ions at about 260 pm constitute the first neighbor shell, a group of eight cesium ions at 450–470 pm form the second-nearest shell, and six sodium ions at 520–550 pm are the third nearest neighbors. It is believed that these strongly electropositive ions screen the central lanthanide ion from the effect of further neighbors. The nearest group of lanthanide ions appears close to 800 pm distant. The substitution of Pr by Sc in the cell affects therefore the fifth nearest neighbor of the lanthanide ion.

The decrease of the lattice parameter should provoke an increase of the Slater parameters, hence an increase of the $^3P_0$ energy due to the combined effect of this electrostatic interaction and the crystal field within $^3H_4$. Instead, a slight decrease of $^3P_0$ is observed, which manifests itself through a lowering of F^2 in all three cases. Besides, when fitted, F^4 increases, but obviously not enough to reverse the trend. The action of the crystal field variation is minor. This explains how but not why the trend in Figure 4 arises. We cannot give any physical reason for this observation.

Table 4. Empirical Hamiltonian parameters of Pr^{3+} in $Cs_2NaPrCl_6$ (CsNaPr), Cs_2NaYCl_6:Pr^{3+} (CsNaY), and $Cs_2NaScCl_6$: Pr^{3+} (CsNaSc) on truncated bases including 23 experimental levels

	$4f^2$ fit			$4f^2 + 4f6p$ fit		
Parameter	CsNaPr	CsNaY	CsNaSc	CsNaPr	CsNaY	CsNaSc
E_{avg}	11,423(12)	11,422(12)	11,428(13)	12,285(37)	12,342(32)	12,393(42)
F^2	67,896(136)	67,781(137)	67,679(144)	67,544(49)	67,458(42)	67,322(56)
F^4	[48,950]	[48,950]	[48,950]	48,321(94)	48,293(83)	48,579(111)
B_0^4 (4f4f)	1917(90)	1963(90)	2017(95)	3444(127)	3645(111)	3802(145)
Simul. B_0^4				*3168*	*3679*	*4501*
B_0^6 (4f4f)	217(43)	228(44)	245(46)	611(37)	673(33)	708(42)
Simul. B_0^6				*504*	*561*	*642*
n_p	4	4	4	5	5	5
σ	41.0	41.4	43.1	13.7	12.0	16.1

The parameters (cm^{-1}) that are held constant are given the same values as for $Cs_2NaPrCl_6$ in Ref. 7. For the $4f^2$ set: $F^6 = 31963$; α, β, $\gamma = 23.5$, -690, 1684, respectively; $M^0 = 2.36$; $\zeta_f = 752.5$; and for the $4f^2 + 4f6p$ set: $F^6 = 31222$; α, β, $\gamma = 22.9$, -698, 2035, respectively; $M^0 = 3.33$; $\zeta_f = 756.1$; $\zeta_p = 3877$; $X = 1.31$. In all cases, $M^2 = 0.56\ M^0$, $M^4 = 0.31\ M^0$; B_0^4 (fp) $= 8.5 \times B_0^4$ (ff), $\Delta E_{avg} = 124{,}000$ (mean difference between the configurations). Standard deviations of the parameters are given between parentheses. $\sigma = \sum_{i=1,\ N}(E_{i_{exp.}} - E_{i_{calc.}})^2/(N - n_p)]^{1/2}$. N, number of energy levels fitted = 23. n_p is the number of parameters. The simulated (Simul.) B_0^4 (ff) and B_0^6 (ff) are given in italics.

Besides, as expected from the decrease of the first neighbor distance, the crystal field parameters increase steadily from the neat to the doped scandium compound. The experimental variation was simulated by a covalent model[12] taking into account the 3s and 3p orbitals of chlorine and assuming ionization energies of Pr^{3+} and Cl^- (3p) equal to $-100{,}000$ and $-125{,}000\ cm^{-1}$, respectively. These values yield crystal field parameters (reported in Table 4) of the same order of magnitude as those fitted from the experiment. Yet, it is obvious that the experimental pace of variation is much lower than the simulated value. From $Cs_2NaPrCl_6$ to $Cs_2NaScCl_6$: Pr^{3+}, the experimental increase of B_0^4 is equal to 5% in $4f^2$, 10% in $4f^2 + 4f6p$, while the variation of the simulated value amounts to 42%. For B_0^6, the variations are smaller: 13%, 16%, and 27%, respectively. Newman[13] in the angular overlap model advocates a R^p power law with p values ranging from 6 to 8. What can be deduced is that the large Pr^{3+} ion when substituted into a lattice site of a smaller ion locally distorts the matrix of the host matrix so that the Pr–Cl distances are larger than the Sc–Cl ones of the host. The host matrix has to accommodate itself to the dopant by the deformation of the first neighbor's shell.

CONCLUSIONS

The $^3P_0$ luminescence of Pr^{3+} in the cubic elpasolite $Cs_2NaScCl_6$ at low concentration ($\sim$0.1 at.%) is well resolved and mainly vibronic in character. At higher concentrations ($\sim$1 at.%), the Pr^{3+} ions do not directly substitute for Sc^{3+} but form other phases. Twenty-three of the $4f^2$ energy levels of $Cs_2NaScCl_6$:Pr^{3+} have been assigned and fitted in an analogous manner to

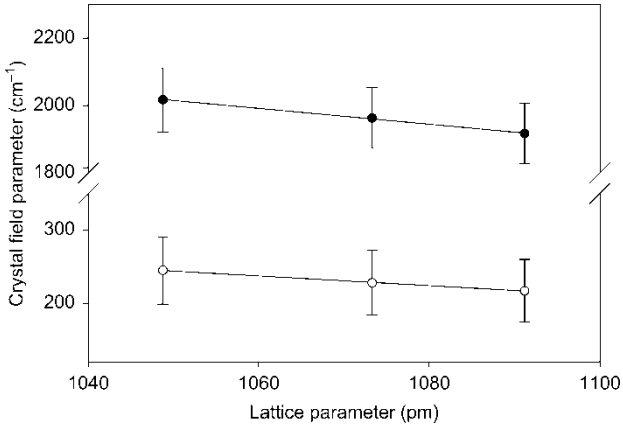

Figure 7. Variation of $4f^2$ crystal field parameters for Cs_2NaMCl_6:Pr^{3+} systems (M = Pr, Y, Sc) with lattice parameter. Upper plot, B_0^4; lower plot, B_0^6. The linear regression lines are shown as a guide to the eye.

those from the spectra of $Cs_2NaYCl_6:Pr^{3+}$ and $Cs_2NaPrCl_6$, where the lattice parameters are greater. The inclusion of configuration interaction of $4f^2$ with an excited configuration of the same parity, 4f6p, greatly improves the crystal field energy level fit. The fitted crystal field parameters from the three systems show the expected trend with lattice parameter. Figure 7 shows the plot of the crystal field parameters derived from the $4f^2$ fit, and a similar variation is observed for the parameters from the CIACF fit. The crystal field parameters have also been simulated by calculation. The comparison with the fitted values shows that the latter do not entirely reflect the rare-earth distance changes from Pr^{3+} to Sc^{3+}. This can be explained by a deformation of the host matrix to accommodate the dopant. It is interesting that the change of the fifth most distant neighbor of Pr^{3+} can have considerable repercussions upon the electronic spectra, the energy level scheme, and the crystal field parameters.

ACKNOWLEDGMENTS

Financial support for this work from the Hong Kong University (Grants Council Research Grant 102304) is gratefully acknowledged.

REFERENCES

1. Meyer, G. The synthesis and structures of complex rare earth halides. *Prog. Solid State. Chem.* **1982**, *14*, 141–219.
2. Oomen, E. W. J. L.; Smit, W. M. A.; Blasse, G. The luminescence of As(III) in the cubic elpasolite $Cs_2NaScCl_6$. *Chem. Phys. Lett.* **1987**, *138*, 584–586.
3. Weaver, S. C.; McClure, D. S. Optical absorption and luminescence spectra of Rh^{3+}-doped Cs_2NaMCl_6 (M = Y, In, Sc) single crystals. *Inorg. Chem.* **1992**, *31*, 2814–2820.
4. Wenger, O. S.; Güdel, H. U. Optical spectroscopy of $CrCl_6^{3-}$ doped $Cs_2NaScCl_6$: broadband near-infrared luminescence and Jahn-Teller effect. *J. Chem. Phys.* **2001**, *114*, 5832–5841.
5. Wenger, O. S.; Valiente, R.; Güdel, H. U. Influence of hydrostatic pressure on the Jahn-Teller effect in the $^4T_{2g}$ excited state of $CrCl_6^{3-}$ doped $Cs_2NaScCl_6$. *J. Chem. Phys.* **2001**, *115*, 3819–3826.
6. Reinhard, C.; Krämer, K.; Biner, D. A.; Güdel, H. U. V^{3+} sensitized upconversion in $Cs_2NaScCl_6:Pr^{3+};V^{3+}$ and $K_2NaScF_6:Er^{3+};V^{3+}$. *J. Alloy. Compd.* **2004**, *374*, 133–136.
7. Tanner, P. A.; Mak, C. S. K.; Faucher, M. D. Configuration interaction of Pr^{3+} in $PrCl_6^{3-}$. *J. Chem. Phys.* **2001**, *114*, 10860–10871.
8. Morss, L. R.; Siegel, M.; Stinger, L.; Edelstein, N. Preparation of cubic chloro complex compounds of trivalent metals. *Inorg. Chem.* **1970**, *9*, 1771–1775.
9. Zissi, G. D.; Papatheodorou, G. N. Changes of vibrational modes upon melting solid $Cs_2NaScCl_6$, Cs_3ScCl_6, $Cs_3Sc_2Cl_9$ and $ScCl_3$. *Chem. Phys. Lett.* **1999**, *308*, 51–57.

10. Tanner, P. A. Spectra, energy levels and energy transfer in high symmetry lanthanide compounds. *Top. Curr. Chem.* **2004**, *241*, 167–278.
11. Tanner, P. A. Electronic spectra of $PrCl_6^{3-}$. *Mol. Phys.* **1986**, *57*, 697–735.
12. Faucher, M.; Garcia, D.; Moune, O. K. Effect of second neighbours on the crystal field in rare earth compounds. *J. Alloy. Compd.* **1992**, *180*, 243–249.
13. Newman, D. J. Power laws for crystal field parameters. *Chem. Phys. Lett.* **1971**, *9*, 606–608.